The $^2\Pi_g$ shape resonance in electron-acetylene scattering: an investigation using the dilated electron propagator method

Arun Venkatnathan, Manoj K. Mishra [1]

Department of Chemistry, Indian Institute of Technology, Bombay, Powai, Mumbai 400 076, India

Abstract

The zeroth order (Σ^0), the second order (Σ^2), the diagonal two particle-one hole Tamm Dancoff approximation ($\Sigma^{2ph\text{-}TDA}$) and the corresponding quasi-particle decouplings of the dilated electron propagator have been used to investigate the $^2\Pi_g$ $C_2H_2^-$ shape resonance. The results compare favourably with the experimental and other theoretical results. A plot of the resonant Feynman–Dyson Amplitudes establishes that the capture of the impinging electron is indeed in the π_g^* orbital of the acetylene molecule. The resonant orbital on the real line shows the attributes of the acetylene lowest unoccupied molecular orbital and for the optimal complex scaling parameter shows a depletion of electron density near the carbon nuclei.

1. Introduction

Resonances are common phenomena in electron-molecule scattering and play an important role in processes involving energy exchange between electronic and nuclear motion. Vibrational excitation of molecules or molecular ions by electron impact, dissociative attachment and recombination are some typically important processes in outer space, in the higher atmosphere and in plasmas and discharges [1,2]. Resonances in which the electron capture is not accompanied by electronic excitation of the target are termed as shape resonances. These resonances can be described as metastable, short-lived anionic complexes which decay, by ejection of an electron, into the target molecule and a scattered electron [3,4].

As acetylene is the prototypical alkyne, the $^2\Pi_g$ $C_2H_2^-$ shape resonance in e-acetylene scattering has been investigated extensively [3–15] and is attributed to a meta-stable electron attachment in its lowest π_g^* orbital. The resonance energy from different experiments have, however, differed considerably [7,11–13] and theoretical calculations [13–15] attempting a full characterization have been scarce, with those by Krumbach et al. [15], employing the Feshbach projection operator formalism coupled with a configuration interaction (CI) stabilisation procedure [16,17], being the most comprehensive. The results so obtained are in excellent agreement with the experimental results and a detailed analysis of the dependence of resonance attributes on basis set, configuration cutoff and stabilization parameters offers important insight. The implementation, however, does depend on the parameter used to control the size of the configuration expansion and the charge perturbation

parameter used to stabilize the resonance. An independent correlated treatment of the $^2\Pi_g$ $C_2H_2^-$ resonance employing a method not dependent on these parameters is, therefore, of obvious utility. Furthermore, since unoccupied orbitals are not invariant in self-consistent field (SCF) calculations, it is useful to independently check the attributes of the resonant orbital and confirm that it is indeed the π_g^* lowest unoccupied molecular orbital (LUMO) that is responsible for the resonant anion formation.

We have recently formulated and implemented a hierarchy of decouplings of the biorthogonal dilated electron propagator method [18,19] where all the electronic co-ordinates in the Hamiltonian are scaled by a complex factor ($\eta = \alpha\, e^{i\theta}$). This permits the use of rigorous complex scaling theorems [20,21] for an accurate characterization of the resonance energy and width and an unequivocal identification of the resonant orbital. This method has been quite useful in the treatment of atomic and molecular shape resonances [22–26]. In this Letter, we present results from an application of the zeroth order, second order, diagonal 2ph-TDA and quasi-particle decouplings of the bi-orthogonal dilated electron propagator [19] to the investigation of the $^2\Pi_g$ $C_2H_2^-$ shape the resonance. The poles and Feynman–Dyson amplitudes (FDAs) from different decouplings and systematically augmented basis sets are examined individually and compared with each other in order to deduce the role of correlation and relaxation in the formation and decay of this resonance.

The formal and computational methodology for the construction and pole search of the biorthogonal dilated electron propagator and the framework for its interpretation are well documented [19] and only the final formulae are collected in the following section. The resonant poles and FDAs from different decouplings of the dilated electron propagator using the basis sets employed by Krumbach et al. [15] and systematically saturated with additional p-orbitals are presented and discussed in Section 3. A summary of the main results concludes this Letter.

2. Method

The electron propagator technique [27,28] is well established and the Dyson equation for the dilated bi-orthogonal matrix electron propagator $\mathbf{G}(\eta, E)$ may again be expressed as [19]

$$\mathbf{G}^{-1}(\eta, E) = \mathbf{G}_0^{-1}(\eta, E) - \mathbf{\Sigma}(\eta, E), \tag{1}$$

where $\mathbf{G}_0(\eta, E)$ is the zeroth order propagator for the uncorrelated electron motion, here chosen as given by the bi-variational SCF approximation [29]. The self energy $\mathbf{\Sigma}(\eta, E)$ matrix incorporates the relaxation and correlation effects.

Solution of the bi-variational SCF equations for the N-electron ground state yields a set of occupied and unoccupied spin orbitals. In terms of these spin orbitals, the matrix elements of $\mathbf{G}_0^{-1}(\eta, E)$ are

$$\left(\mathbf{G}_0^{-1}(\eta, E)\right)_{ij} = (E - \epsilon_i)\,\delta_{ij}, \tag{2}$$

where ϵ_i is the orbital energy corresponding to the ith spin orbital. Through the second order of electron interaction, the elements of the self-energy matrix are [19]

$$\Sigma_{ij}^2(\eta, E) = \tfrac{1}{2} \sum_{k,l,m} N_{klm} \frac{\langle ik \,\|\, lm\rangle \langle lm \,\|\, jk\rangle}{(E + \epsilon_k - \epsilon_l - \epsilon_m)} \tag{3}$$

where

$$N_{klm} = \langle n_k\rangle - \langle n_k\rangle\langle n_l\rangle - \langle n_k\rangle\langle n_m\rangle + \langle n_l\rangle\langle n_m\rangle \tag{4}$$

with $\langle n_k\rangle$ being the occupation number for the kth spin orbital and the antisymmetric two-electron integral

$$\langle ij \,\|\, kl\rangle = \eta^{-1} \int \psi_i(1)\,\psi_j(2)\left[(1 - P_{12})/r_{12}\right] \times \psi_k(1)\,\psi_l(2)\,\mathrm{d}x_1\mathrm{d}x_2\,. \tag{5}$$

The lack of complex conjugation stems from the bi-orthogonal set of orbitals, resulting from bi-variational SCF, being the complex conjugate of each other [29,30]. For the diagonal 2ph-TDA [27,28] decoupling of the dilated electron propagator [24]

$$\Sigma_{ij}^{\text{2ph-TDA}}(\eta, E) = \tfrac{1}{2} \sum_{k,l,m} N_{klm} \times \frac{\langle ik \,\|\, lm\rangle \langle lm \,\|\, jk\rangle}{(E + \epsilon_k - \epsilon_l - \epsilon_m) - \Delta}, \tag{6}$$

where

$$\Delta = \tfrac{1}{2}\langle ml \,\|\, ml\rangle\big(1 - \langle n_m\rangle - \langle n_l\rangle\big) - \langle km \,\|\, km\rangle \times \big(\langle n_k\rangle - \langle n_m\rangle\big) - \langle kl \,\|\, kl\rangle\big(\langle n_k\rangle - \langle n_l\rangle\big)\,. \tag{7}$$

In terms of the spin-orbitals obtained from the bi-variational SCF procedure, combining Eqs. (1) and (2) we may write the matrix electron propagator as

$$\mathbf{G}^{-1}(\eta,E) = E\mathbf{1} - \boldsymbol{\epsilon}(\eta) + \boldsymbol{\Sigma}(\eta,E) = E\mathbf{1} - \mathbf{L}(\eta,E) \quad (8)$$

or, in operator form

$$G(\eta,E) = (E - L(\eta,E))^{-1} \quad (9)$$

where, in terms of the eigenfunctions and eigenvalues of $L(\eta,E)$

$$L(\eta,E)\,\boldsymbol{\chi}_n(\eta,E) = \mathscr{E}_n(\eta,E)\,\boldsymbol{\chi}_n(\eta,E)\,. \quad (10)$$

The spectral representation of G is given by

$$G(\eta,E) = (E - L(\eta,E))^{-1} \sum_n |\chi_n\rangle\langle\chi_n| = \sum_n \frac{|\chi_n\rangle\langle\chi_n|}{E - \mathscr{E}_n(\eta,E)} \quad (11)$$

and the eigenvalues of L therefore represent the poles of G. Accordingly, the usual dilated electron propagator calculations proceed by iterative diagonalization

$$\mathbf{L}(\eta,E)\,\boldsymbol{\chi}_n(\eta,E) = \mathscr{E}_n(\eta,E)\,\boldsymbol{\chi}_n(\eta,E) \quad (12)$$

with

$$\mathbf{L}(\eta,E) = \boldsymbol{\varepsilon} + \boldsymbol{\Sigma}(\eta,E) \quad (13)$$

where $\boldsymbol{\varepsilon}$ is the diagonal matrix of the orbital energies and $\boldsymbol{\Sigma}$ is the self energy matrix. The propagator pole $\mathscr{E}$ is obtained by repeated diagonalizations such that one of the eigen-values $\mathscr{E}_n(\eta,E)$ of $\mathbf{L}(\eta,E)$ fulfills the condition $E = \mathscr{E}_n(\eta,E)$ [19]. These $\mathscr{E}_n(\eta,E)$ represent the poles of the dilated electron propagator G(η,E). From among these poles, the resonant pole $\mathscr{E}_r(\eta,E)$ and the corresponding eigenvector (FDA) $\chi_r(\eta,E)$ are selected as per the prescription of the complex scaling theorems [20,21] wherein those roots in the continua which are invariant to changes in the complex scaling parameter η are to be associated with resonances. In a limited basis set calculation, instead of absolute stability one finds quasi-stability where the θ trajectory displays kinks, cusps, loops or inflections which indicate the proximity of a stationary point [31] and in our case the resonance attributes have been extracted from the value at the kink in θ-trajectories ($\partial\mathscr{E}_r/\partial\theta = 0$). The real part of the resonant pole furnishes the energy and the imaginary part the half width of the resonance.

The quasiparticle approximation [32] for the dilated electron propagator [26] results from a diagonal approximation to the self-energy matrix $\boldsymbol{\Sigma}(\eta,E)$ with poles of the dilated electron propagator given by

$$E(\eta) = \epsilon_i + \Sigma_{ii}(\eta,E) \quad (14)$$

which are determined iteratively beginning with $E = \epsilon_i$ and Σ_{ii} may correspond to any perturbative (Σ^2) or renormalised decoupling such as the diagonal $\Sigma^{2\text{ph-TDA}}$.

In the bi-variationally obtained bi-orthogonal orbital basis $\{\psi_i\}$, the FDA χ_n is a linear combination

$$\chi_n(\mathbf{r}) = \sum_i C_{ni}\psi_i(\mathbf{r}) \quad (15)$$

where the mixing of the canonical orbitals allows for the incorporation of correlation and relaxation effects. In the zeroth ($\boldsymbol{\Sigma} = \mathbf{0}$) and quasi-particle approximations (diagonal $\boldsymbol{\Sigma}$), there is no mixing. The difference between perturbative second order (Σ^2) or renormalized diagonal 2ph-TDA ($\Sigma^{2\text{ph-TDA}}$) decouplings manifests itself through the differences between the mixing coefficients C_{ni} from these approximations.

3. Results and discussion

The primitive contracted Gaussian-type orbital (CGTO) bases employed in our calculations are those used earlier by Krumbach et al. [15]. The 56 CGTO basis (I) utilizes the 5s5p1d CGTOs on C-atoms and 2s CGTOs on H-atoms. The 76 CGTO basis (II) utilizes the 5s6p1d CGTOs on C-atoms and 3s2p CGTOs on H-atoms. The 76 CGTO basis was saturated systematically to the linear dependency limit by first adding an extra uncontracted p orbital on the C atom, one at a time, with the exponent of this new p-type CGTO being one half of the lowest exponent of the previous set and then by adding an additional uncontracted p orbital on the H atom with the lowest p type GTO exponent of the 3s2p CGTO basis (II) centered on the H-atom being scaled by 0.25. The CGTO basis sets so obtained were those with 5s7p1d on C and 3s2p on H (III), 5s8p1d on C and 3s2p on H (IV), 5s9p1d on C and 3s2p on H (V) and 5s9p1d

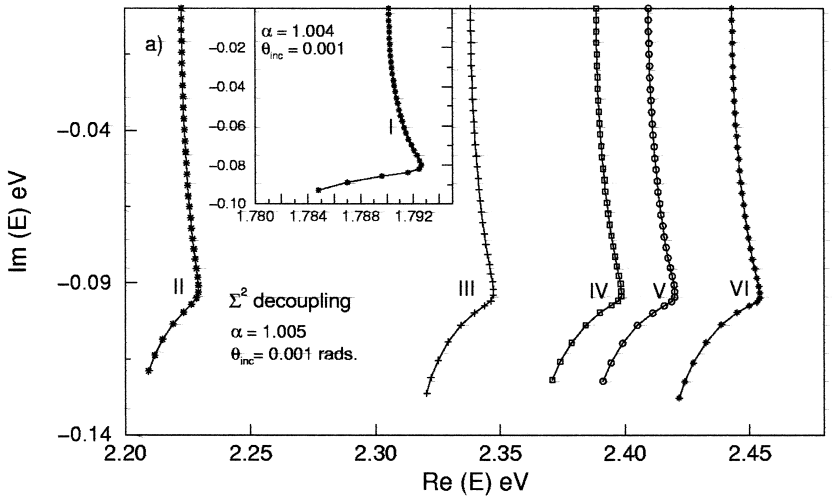
a)
α = 1.004
θinc = 0.001
I
II
III
IV
V
VI
Σ² decoupling
α = 1.005
θinc= 0.001 rads.
Im (E) eV
Re (E) eV

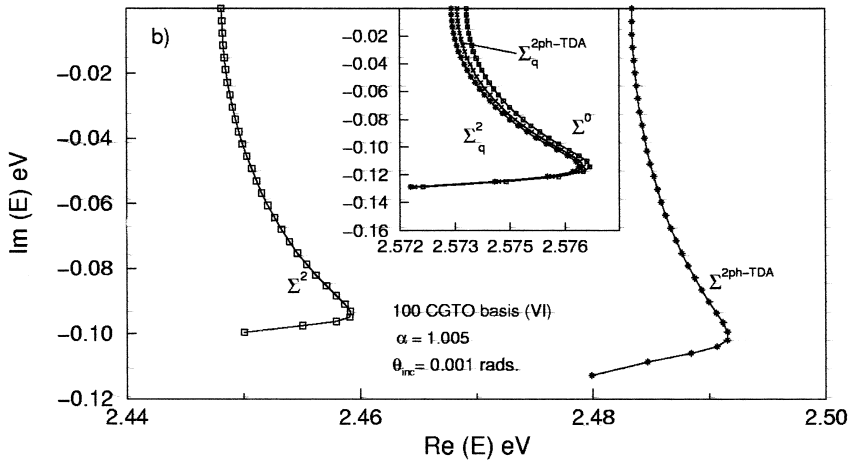
b)
Σq2ph-TDA
Σq²
Σ⁰
Σ²
Σ2ph-TDA
100 CGTO basis (VI)
α = 1.005
θinc= 0.001 rads.
Im (E) eV
Re (E) eV

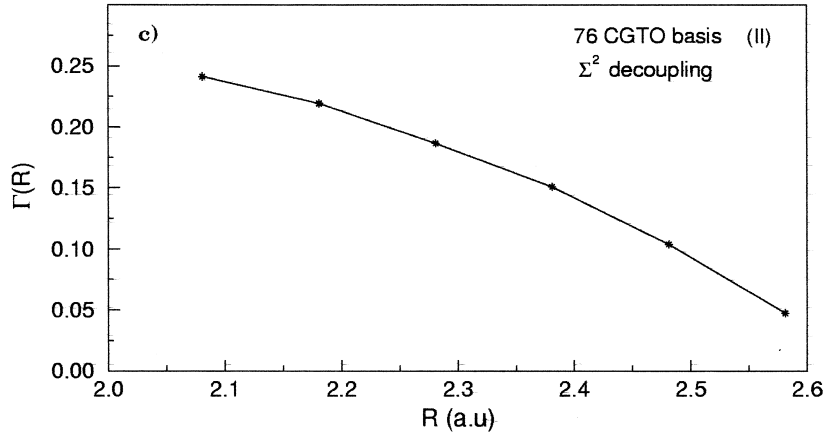
c)
76 CGTO basis (II)
Σ² decoupling
Γ(R)
R (a.u)

Table 1
Energy and width of the $^2\Pi_g$ shape resonance in e-C_2H_2 scattering

Method/reference	Energy (eV)	Width (eV)
Experiment:		
Trapped electron [6,7]	1.8/1.85	–
Vibrational Excitation [8]	2.6	> 1.0
Electron impact [9]	2.5	1.0
Dissociative attachment [10]	3.0	0.6
Theory:		
Multiple-Scattering X α [13]	2.6	1.0
MNDO [14]	1.7–2.2	–
CI {I/II} [15]	3.29/2.92	1.1 / 1.1
Results from Biorthogonal Dilated Electron Propagator (this work) {I/II/III/IV/V/VI}		
Zeroth Order	1.84/2.32/2.45/2.51/2.53/2.58	0.14/0.21/0.23/0.23/0.23/0.23
Second Order	1.79/2.23/2.35/2.40/2.42/2.46	0.16/0.19/0.19/0.19/0.19/0.19
Quasiparticle second order	1.84/2.32/2.45/2.51/2.53/2.58	0.16/0.21/0.23/0.23/0.23/0.23
Diagonal 2ph-TDA	1.81/2.26/2.38/2.43/2.45/2.49	0.16/0.20/0.20/0.20/0.20/0.20
Quasiparticle Diagonal 2ph-TDA	1.84/2.32/2.45/2.51/2.53/2.58	0.13/0.20/0.23/0.23/0.23/0.23

1 (5s5p1d on C/2s on H). II (5s6p1d on C/3s2p on H). III (5s7p1d on C/3s2p on H). IV (5s8p1d on C/3s2p on H). V (5s9p1d on C/3s2p on H). VI (5s9p1d on C/3s3p on H).

on C and 3s3p on H (VI). Theta trajectories [31] from the second order (Σ^2) decoupling of the dilated electron propagator utilizing all these bases (I–VI) are plotted in Fig. 1a. Theta trajectories from different decouplings of the dilated electron propagator employing the saturated 100 CGTO basis are plotted in Fig. 1b. The resonance energies and widths are extracted from the quasi-stable portion of these trajectories for the optimal θ value (θ_{opt}) corresponding to the inflection in the theta trajectories. The real part of the resonant root at optimal theta furnishes the resonance energy and the imaginary part the half width of the resonance and these values are collected in Table 1 along with those from other experimental and theoretical methods. The zeroth (Σ^0), the quasi-particle second order (Σ_q^2) and the quasi-particle diagonal 2ph-TDA ($\Sigma_q^{2\text{ph-TDA}}$) decouplings do not allow mixing and the inset in Fig. 1b shows that a lack of orbital mixing in the Σ^0, Σ_q^2, $\Sigma_q^{2\text{ph-TDA}}$ decouplings leads to a higher value for the resonance energy.

The results collected in Table 1 show that, unlike the case of CI calculations [15], both the resonance energy and the width calculated using basis (I) is lower in comparison to those calculated with basis (II) for all the decouplings. This behaviour (where results from the larger basis are higher than those from the smaller basis) is contrary to the variational principle and requires an explanation. We note that the dilated electron propagator method employed in our investigation is a many body perturbation theoretic approach and is not variational in nature. Since resonances correspond to a continuum root, at the SCF (zeroth order) level these are mimicked by a resonant virtual orbital energy identified as per the complex scaling prescription detailed earlier. In our case, the perturbative/renormalized self energy approximations provide a correction to the resonant

Fig. 1. Theta trajectories from (a) second order decoupling of the dilated electron propagator using the CGTO bases I–VI; (b) different decouplings using basis (VI), and c) width vs C–C bond distance from second order decoupling using basis (II). The trajectories start on the real line ($\theta = 0$) and θ increments are in steps (θ_{inc}) of 0.001 radians.

virtual orbital energy which is not invariant in the SCF scheme and whose basis-set dependence cannot be controlled and has no variational bound. The perturbative second order and other self energy corrections are also non-variational. Therefore the basis set trends need not be variational and this non-variational behaviour is seen in our results. This indicates that basis sets should be systematically saturated before the results for resonance energies can be taken to be authentic. As will be shown later, the larger basis provides a more diffuse resonant orbital, with a greater electron density away from the nucleus, which we believe to be the reason for the higher resonance energy from the larger basis. This further underscores the need for a systematic augmentation of basis sets if reliable results are to be obtained.

That the larger 76 CGTO basis (II) used by Krumbach et al. [15] needs further saturation is seen from the 0.25 eV difference in the resonance energy value obtained from bases (II) and (VI). For all the bases, the correlated decouplings lower both the resonance energy and width. In keeping with the general trends seen in our previous calculations on molecular resonances [19,25,26], the Σ^2 decoupling seems to incorporate a higher level of correlation and relaxation (compared to $\Sigma^{2\text{ph-TDA}}$) since the lowering of both the resonance energy and the width vis-a-vis the values from the Σ^0 decoupling is larger in this case. The basis set effect is much larger than that of the correlation/relaxation incorporated by higher order decouplings. The resonance energy from the smallest and the largest basis sets differ from each other by as much as 0.74 eV in comparison to the much smaller difference from different decouplings using the same basis set. Basis set saturation is therefore of obvious importance.

All the earlier calculations [19] using the dilated electron propagator technique have been for a single equilibrium value of the internuclear distance. The variation of width as a function of the C–C bond length is plotted in Fig. 1c. As expected, since electron attachment is in the antibonding π_g^* orbital, an increase in the C–C bond length stabilizes the metastable anion leading to a narrowing of width as a function of the C–C stretch. The calculated widths are, however, much narrower than those from other calculations and experiments but this display of qualitatively correct behaviour engenders a hope that the use of $E_{(A^-)^*}(R) = E_A(R) + \varepsilon_{\text{res}}(R)$ as the complex potential energy curve for the metastable anion $(A^-)^*$ dynamics to calculate vibrational structure may become feasible in the future, with appropriate corrections brought in by the higher order decouplings.

The use of FDAs as correlated orbitals from the Σ^2 decoupling for the largest 100 CGTO (VI) basis for $\theta = 0.0$ and $\theta = \theta_{\text{opt}} = 0.027$ radians (the value corresponding to the inflection in the theta trajectory associated with resonance formation) are plotted in Figs. 2a–c. The imaginary part of the FDA at $\theta = \theta_{\text{opt}}$ is an order of magnitude smaller than the real part. The difference in the probability density profile resulting from resonance formation at $\theta = \theta_{\text{opt}}$ has been plotted in Fig. 2d and reveals a very small ($\approx 10^{-4}$) but uniform depletion of electron density from the vicinity of the carbon nuclei. For the large 100 CGTO basis (VI) employed here, the complex scaling parameter ($\eta = \alpha\, e^{i\theta}$) plays only a minimal role ($\alpha_{\text{opt}} = 1.005$ and $\theta_{\text{opt}} = 0.027$ radians) of identifying the resonant root and bringing it in the complex plane making the corresponding FDA slightly more diffuse by depleting electron density from the vicinity of the carbon nuclei.

The basis set effect is considerably large and to explore the role of additional diffuse functions added to the 76 CGTO basis used by Krumbach et al. [15] we have plotted the difference between the resonant Feynman–Dyson amplitudes for $\theta = 0.0$ and $\theta = \theta_{\text{opt}}$(0.027 radians) in Figs. 3a and 3b respectively. In conjunction with the FDA profiles of Figs. 2a and 2b it can be seen that additional diffuse functions on C and H atoms provides a uniform increase in the probability amplitude around the whole C_2H_2 molecule making the 100 CGTO resonant FDA more diffuse compared to the resonant FDA from the 76 CGTO basis, both on the real line and for $\theta = \theta_{\text{opt}} =$ 0.027 radians. That this overall change in amplitude profile with additional basis functions is more important than correlation effects brought in by incorporating the higher order decouplings is seen from the difference between the FDAs from the second order (Σ^2) and zeroth order (Σ^0) (the complex scaled bi-variational SCF) and the difference between the (Σ^2) and diagonal 2ph-TDA ($\Sigma^{2\text{ph-TDA}}$) decouplings plotted in Figs. 3c and 3d respectively. Even

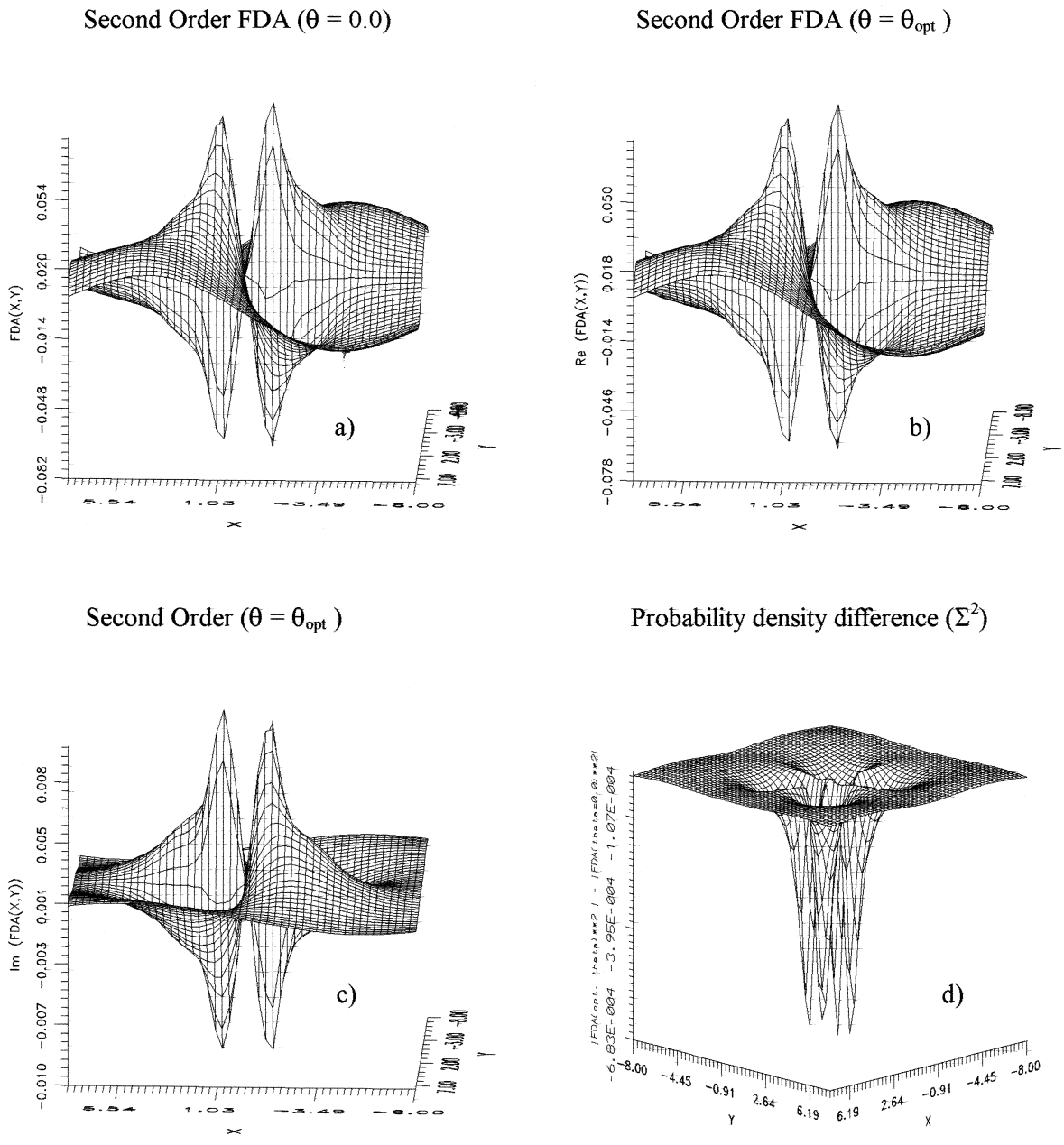

Fig. 2. The Feynman–Dyson amplitude (FDA) from the second order decoupling using basis (VI) for (a) $\alpha = 1.005$ at $\theta = 0$; (b) the real part; (c) the imaginary part for $\theta = \theta_{opt} = 0.027$ radians, and (d) the difference between the probability densities from the Σ^2 FDA at $\theta = \theta_{opt}$ and $\theta = 0$ using basis (VI).

though the decoupling related difference (Fig. 3c) is larger than that ensuing from a basis-set saturation (Figs. 3a and 3b) the decoupling related effect on the resonance energy is much less ($\varepsilon^2 - \varepsilon^0 \approx 0.13$ eV) compared with that from basis set ($\varepsilon^2_{VI} - \varepsilon^2_{II} = 0.26$). The widths are much less sensitive to either the decoupling effects or the basis set variations with the differences being numerically insignificant.

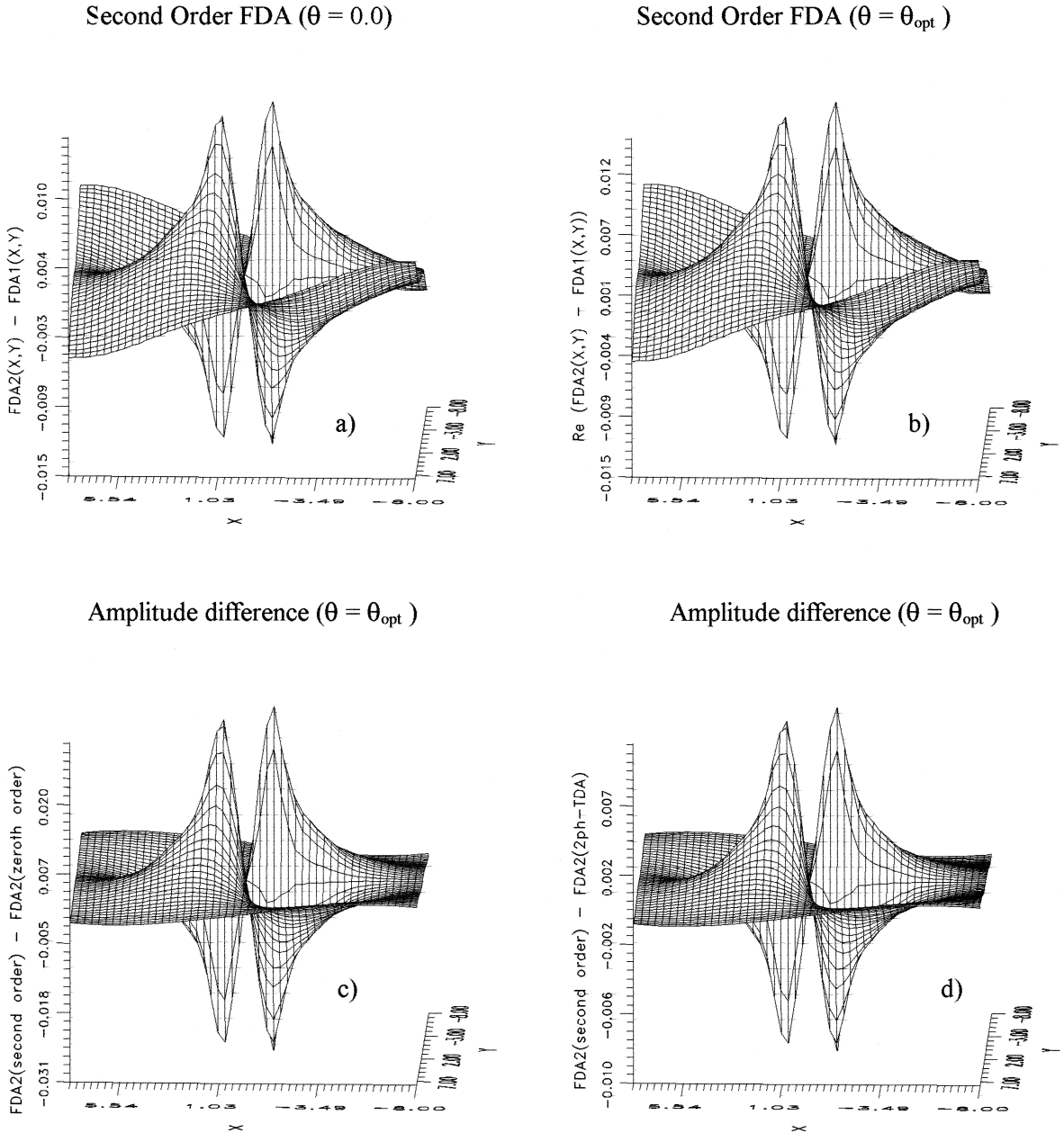

Fig. 3. The difference between the real part of the FDA from the Σ^2 decoupling using bases (VI) and (II) for (a) $\alpha = 1.005$ at $\theta = 0$ and (b) $\theta = \theta_{opt} = 0.027$ radians. (c) The real part of the difference at $\theta = \theta_{opt}$ between the Σ^2 and Σ^0 decouplings and (d) between the Σ^2 and $\Sigma^{2ph\text{-}TDA}$ decouplings using basis (VI).

The role of correlation and relaxation may be assessed from Figs. 3c and 3d where it can be seen that the resonant FDA from the Σ^2 decoupling brings a greater amount of amplitude near the C–C bond region in comparison with the resonant FDAs from both the Σ^0 and the $\Sigma^{2ph\text{-}TDA}$ decouplings, thereby lowering the resonance energy of the $^2\Pi_g$ $C_2H_2^-$ resonance. That the Σ^2 decoupling is a

better approximation than the numerically more demanding diagonal $\Sigma^{2ph\text{-}TDA}$ one is seen in Fig. 3d which displays a buildup of extra electron density on both the carbon atoms by the Σ^2 FDA.

4. Concluding remarks

Our investigation of the $^2\Pi_g$ $C_2H_2^-$ shape resonance in electron-acetylene scattering, using the dilated electron propagator method based on the bi-variational SCF has led to the confirmation of the acetylene π_g^* LUMO as the resonant orbital. The complex scaling parameter provides an unequivocal identification of the resonant root corresponding to metastable electron attachment and provides an additional mechanism for redistribution of electron density around the carbon nuclei. The description of resonances is extremely sensitive to the choice of the primitive basis employed. The effect on the resonance attributes can be seen by comparing the results from the 100 CGTO basis (which provides results closer to the experimental resonance energy) and the lowest 56 CGTO basis. These results differ by as much as 0.7 eV.

The bi-variational SCF (Σ^0) and the diagonal quasi-particle decouplings (Σ_q^2 and $\Sigma_q^{2ph\text{-}TDA}$) do not permit any mixing of orbitals. A comparison of resonance energy from these decouplings with those from Σ^2 and $\Sigma^{2ph\text{-}TDA}$ decouplings shows that orbital relaxation has a significant role in molecular resonance formation. Maximum lowering and stabilization of the $^2\Pi_g$ $C_2H_2^-$ resonance is effected through the accumulation of the orbital amplitude near the carbon nuclei by the second order (Σ^2) decoupling. Although the numerically more demanding diagonal 2ph-TDA approximation is supposed to provide a renormalized summation of the most important diagonal ring and ladder diagrams to all orders, it offers little or no advantage vis-a-vis the Σ^2 decoupling. The width of the $^2\Pi_g$ $C_2H_2^-$ resonance calculated by us, even with the largest basis employed here, is once again much smaller than those from other methods and this extra stability (longer lifetime) implies that correlation due to inter-electronic repulsions is probably not accommodated adequately by the decouplings developed so far. To us, this indicates a need for the third and higher order decouplings which shall be the focus of our future activities.

Acknowledgements

We are pleased to acknowledge financial support from the Department of Science and Technology, India (grant No. SP/S1/H26/96).

References

[1] H. Massey, Negative Ions, Cambridge Univ. Press, London, 1976.
[2] J.N. Bardsley, M.A. Biondi, Adv. At. Mol. Phys. 6 (1971) 1.
[3] K.D. Jordan, P.D. Burrow, Acc. Chem. Res. 11 (1978) 341.
[4] K.D. Jordan, P.D. Burrow, Chem. Rev. 87 (1987) 557.
[5] C.R. Bowman, W.D. Miller, J. Chem. Phys. 42 (1965) 681.
[6] D.F. Dance, I.C. Walker, Chem. Phys. Lett. 18 (1973) 601.
[7] E.H. Van Veen, F.L. Plantenga, Chem. Phys. Lett. 38 (1976) 493.
[8] K.H. Kochem, W. Sohn, K. Jung, H. Erhardt, E.S. Chang, J. Phys. B: At. Mol. Phys. 18 (1985) 1253.
[9] L. Andric, R.I. Hall, J. Phys. B: At. Mol. Phys. 21 (1988) 355.
[10] R. Dressler, H. Allan, J. Chem. Phys. 87 (1987) 4510.
[11] G.J. Schulz, Phys. Rev. 112 (1958) 150.
[12] D.F. Dance, I.C. Walker, J. Chem. Soc., Faraday Trans. 70 (1974) 1426.
[13] J.A. Tossel, J. Phys. B: At. Mol. Phys. 18 (1985) 387.
[14] J. Chandrasekhar, R.A. Kahn, P.R. Schleyer, Chem. Phys. Lett. 85 (1982) 493.
[15] V. Krumbach, B.M. Nestmann, S.D. Peyerimhoff, J. Phys. B: At. Mol. Phys. 22 (1989) 4001.
[16] B.M. Nestmann, S.D. Peyerimhoff, J. Phys. B: At. Mol. Phys. 18 (1985) 615.
[17] B.M. Nestmann, S.D. Peyerimhoff, J. Phys. B: At. Mol. Phys. 18 (1985) 4309.
[18] M.K. Mishra, M.N. Medikeri, A. Venkatnathan, S. Mahalakshmi, Mol. Phys. 94 (1998) 127.
[19] M.K. Mishra, M.N. Medikeri, Adv. Quantum Chem. 27 (1996) 223.
[20] W.P. Reinhardt, Ann. Rev. Phys. Chem. 33 (1982) 223.
[21] B.R. Junker, Adv. At. Mol. Phys. 18 (1982) 207.
[22] M.K. Mishra, H.A. Kurtz, O. Goscinski, Y. Öhrn, J. Chem. Phys. 79 (1983) 1896.
[23] M.K. Mishra, O. Goscinski, Y. Öhrn, J. Chem. Phys. 79 (1983) 5494.
[24] M.N. Medikeri, J. Nair, M.K. Mishra, J. Chem. Phys. 99 (1993) 1869.
[25] M.N. Medikeri, M.K. Mishra, J. Chem. Phys. 100 (1994) 2044.
[26] M.N. Medikeri, M.K. Mishra, Chem. Phys. Lett. 211 (1993) 607.

[27] W. von Niessen, J. Schirmer, L.S. Cederbaum, Comp. Phys. Rept. 1 (1984) 57.
[28] Y. Öhrn, G. Born, Adv. Quantum Chem. 13 (1981) 1.
[29] P.O. Löwdin, P. Froelich, M.K. Mishra, Adv. Quantum Chem. 20 (1989) 185.
[30] M.K. Mishra, Y. Öhrn, P. Froelich, Phys. Lett. A. 81 (1981) 4.
[31] N. Moiseyev, S. Friedland, P.R. Certain, J. Chem. Phys. 74 (1981) 4739.
[32] L.S. Cederbaum, Theoret. Chim. Acta. 31 (1973) 239.